Enhanced four-wave mixing efficiency in four-subband semiconductor quantum wells via Fano-type interference

Shaopeng Liu,[1] Wen-Xing Yang,[1,2*] You-Lin Chuang,[2] Ai-Xi Chen,[3] Ang Liu,[1] Yan Huang,[4] and Ray-Kuang Lee[2]

[1]*Department of Physics, Southeast University, Nanjing 210096, China*
[2]*Institute of Photonics Technologies, National Tsing-Hua University, Hsinchu 300, Taiwan*
[3]*Department of Applied Physics, School of Basic Science, East China Jiaotong University, Nanchang 330013, China*
[4]*School of Electronic Science and Engineering, Southeast University, Nanjing 210096, China*
[*]*wenxingyang@seu.edu.cn*

Abstract: We propose and analyze an efficient way to enhance four-wave mixing (FWM) signals in a four-subband semiconductor quantum well via Fano-type interference. By using Schrödinger-Maxwell formalism, we derive explicitly analytical expressions for the input probe pulse and the generated FWM field in linear regime under the steady-state condition. With the aid of interference between two excited subbands tunneling to the common continuum, the efficiency to generate FWM field is found to be significantly enhanced, up to 35%. More interestingly, a linear growth rate in the FWM efficiency is demonstrated as the strength of Fano-type interference increases in presence of the continuum states, which can be maintained for a certain propagation distance (i.e., 50μm).

OCIS codes: (190.5970) Semiconductor nonlinear optics including MQW; (190.4380) Nonlinear optics, four-wave mixing.

References and links

1. S. E. Harris and L. V. Hau, "Nonlinear optics at low light levels," Phys. Rev. Lett. **82**, 4611–4614 (1999).
2. M. Fleischhauer, A. Imamoglu, and J.P. Marangos, "Electromagnetically induced transparency: Optics in coherent media," Rev. Mod. Phys. **77**, 633–673 (2005).
3. S. E. Harris, "Lasers without inversion: interference of lifetime-broadened resonances," Phys. Rev. Lett. **62**, 1033–1036 (1989).
4. L. V. Hau, S. E. Harris, Z. Dutton, and C.H. Behroozi, "Light speed reduction to 17 metres per second in an ultracold atomic gas," Nature (London) **397**, 594–598 (1999).
5. L. J. Wang, A. Kuzmich, and A. Dogariu, "Gain-assisted superluminal light propagation," Nature (London) **406**, 277–279 (2000).
6. Y. Wu and L. Deng, "Achieving multifrequency mode entanglement with ultraslow multiwave mixing," Opt. Lett. **29**, 1144–1146 (2004).
7. A. B. Matsko, I. Novikova, G. R. Welch, and M. S. Zubairy, "Enhancement of Kerr nonlinearity by multiphoton coherence," Opt. Lett. **28**, 96–98 (2003).
8. Y. Wu, M. G. Payne, E. W. Hagley, and L. Deng, "Efficient multiwave mixing in the ultraslow propagation regime and the role of multiphoton quantum destructive interference," Opt. Lett. **29**, 2294–2296 (2004).
9. W. X. Yang, J. M. Hou, and R.-K. Lee, "Ultraslow bright and dark solitons in semiconductor quantum wells," Phys. Rev. A **77**, 033838 (2008).
10. W. X. Yang, J. M. Hou, Y. Y. Lin, and R.-K. Lee, "Detuning management of optical solitons in coupled quantum wells," Phys. Rev. A **79**, 033825 (2009).

#223802 - $15.00 USD Received 26 Sep 2014; revised 26 Oct 2014; accepted 2 Nov 2014; published 14 Nov 2014

11. W. X. Yang, A. X. Chen, R.-K. Lee, and Y. Wu, "Matched slow optical soliton pairs via biexciton coherence in quantum dots," Phys. Rev. A **84**, 013835 (2011).
12. H. Sun, Y. Niu, R. Li, S. Jin, and S. Gong, "Tunneling-induced large cross-phase modulation in an asymmetric quantum well," Opt. Lett. **32**, 2475–2477 (2007).
13. J. H. Wu, J. Y. Gao, J. H. Xu, L. Silvestri, M. Artoni, G. C. LaRocca, and F. Bassani, "Ultrafast all optical switching via tunable Fano interference," Phys. Rev. Lett. **95**, 057401 (2005).
14. J. Li, "Controllable optical bistability in a four-subband semiconductor quantum well system," Phys. Rev. B **75**, 155329 (2007)
15. W. X. Yang, J. M. Hou, and R.-K. Lee, "Highly efficient four-wave mixing via intersubband transitions in InGaAs/AlAs coupled double quantum well structures," J. Mod. Opt. **56**, 716–721 (2009).
16. P. R. Hemmer, D. P. Katz, J. Donoghue, M. Cronin-Golomb, M. S. Shahriar, and P. Kumar, "Efficient low-intensity optical phase conjugation based on coherent population trapping in sodium," Opt. Lett. **20**, 982–984 (1995).
17. H. C. Liu and F. Capasso, *Intersubband Transitions in Quantum Wells: Physics and Device Applications* (Academic, New York, 2000), pp. 5–18.
18. J. Faist, F. Capasso, C. Sirtori, K. W. West, and L. N. Pfeiffer, "Controlling the sign of quantum interference by tunnelling from quantum wells," Nature **390**, 589–591 (1997).
19. H. Schmidt, K. L. Campman, A. C. Gossard, A. Imamoglu, "Tunneling induced transparency: Fano interference in intersubband transitions," Appl.Phys. Lett. **70**, 3455–3457 (1997).
20. X. Hao, J. Li, J. Liu, P. Song, and X. Yang, "Efficient four-wave mixing of a coupled double quantum-well nanostructure," Phys. Lett. A **372**, 2509–2513 (2008).
21. X. Hao, J. Li, and X. Yang, "Mid-infrared efficient generation by resonant four-wave mixing in a three-coupled-quantum-well nanostructure," Opt. Commun. **282**, 3339–3344 (2009).
22. H. Sun, S. Fan, H. Zhang, and S. Gong, "Tunneling-induced high-efficiency four-wave mixing in asymmetric quantum wells," Phys. Rev. B **87**, 235310 (2013).
23. G. B. Serapiglia, E. Paspalakis, C. Sirtori, K. L. Vodopyanov, and C. C. Phillips, "Laser-induced quantum coherence in a semiconductor quantum well," Phys. Rev. Lett. **84**, 1019–1022 (2000).
24. T. Müller, W. Parz, G. Strasser, K. Unterrainer, "Influence of carrier-carrier interaction on time-dependent intersubband absorption in a semiconductor quantum well," Phys. Rev. B **70**, 155324 (2004).
25. J. F. Dynes, M. D. Frogley, M. Beck, J. Faist, and C. C. Phillips, "Ac stark splitting and quantum interference with intersubband transitions in quantum wells," Phys. Rev. Lett. **94**, 157403 (2005).
26. M. Wagner, H. Schneider, D. Stehr, S. Winnerl, A. M. Andrews, S. Schartner, G. Strasser, and M. Helm, "Observation of the intraexciton Autler-Townes effect in GaAs/AlGaAs semiconductor quantum wells," Phys. Rev. Lett. **105**, 167401 (2010).
27. Y. Wu and X. Yang,"Highly efficient four-wave mixing in double-Λ system in ultraslow propagation regime," Phys. Rev. A **70**, 053818 (2004).

Over the past few decades, quantum interference in the form of electromagnetically induced transparency (EIT) has attracted tremendous interests in optical communications and quantum information processing [1,2]. This concept of quantum interference is also extended to a variety of applications, including lasing without inversion [3], controlling the group velocity of light pulses [4, 5], and highly efficient schemes for nonlinear optics [6–8]. For examples, nonlinear optical phenomena based on the quantum interference have been demonstrated for optical solitons [9–11], enhanced nonlinearity [12–14], and multi-wave mixing processes in the ultraslow propagation regime [15, 16]. In particular, multi-wave mixing process is expected to have a wide range of applications in diverse fields, such as generation of short-wavelength coherent radiation, nonlinear spectroscopy with low-light intensity, quantum single-photon nonlinear optics, and quantum information science. However, the low conversion efficiency for multi-wave mixing in ultraslow propagation regime limits its applications.

In addition to the atomic media, quantum interference phenomena associated with intersubband transitions (ISBT) in semiconductor quantum wells (SQW) have also been utilized based on the analogue between atomic and electronic energy levels [17]. One advantage in the SQW system is the more accessible Fano-type interference, which arises from the absorption paths of two states coupled to a common continuum and leads to nonreciprocal absorptive and dispersive profiles [18, 19]. In this work, with the aid of interference between two excited subbands tunneling to the common continuum, we propose and analyze an efficient way to enhance four-

#223802 - $15.00 USD Received 26 Sep 2014; revised 26 Oct 2014; accepted 2 Nov 2014; published 14 Nov 2014

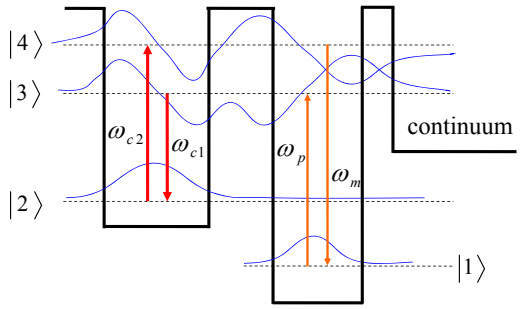

Fig. 1. Schematic band diagram of our asymmetric double SQW structure with a four-subband $|j\rangle$ ($j = 1-4$) configuration. Here, Fano-type interference occurs in the optical absorption from the ground state $|1\rangle$ to two continuum resonant states $|3\rangle$ and $|4\rangle$. Related energy levels and the corresponding wave functions are denoted by dashed- and solid-lines, respectively. The SQW structure interacts with two continuous-wave (cw) pump lasers (frequencies ω_{c1}, ω_{c2} and Rabi frequencies $2\Omega_{c1}$, $2\Omega_{c2}$) and a probe pulse (frequency ω_p and Rabi frequency $2\Omega_p$), in order to generate a new FWM pulse field (frequency ω_m and Rabi frequency $2\Omega_m$).

wave mixing (FWM) signals in SQW with a four -subband configuration. Different from using quantum destructive interference induced by the continuous-wave (cw) control field [20, 21] or the resonant tunneling [22], our scheme based on one weak probe pulse interacting with two cw pump fields is analyzed for the enhanced FWM generation. By solving the coupled Schrödinger-Maxwell equations, a time-dependent analysis in the ultraslow propagation regime is performed for the generated FWM field. We show the corresponding analytical expressions explicitly, for the probe and generated FWM pulses, as well as their phase shifts, absorption coefficients, group velocities, and the related conversion efficiency, respectively. Owing to the existence of Fano-type interference, our results illustrate the possibility to have a maximum FWM conversion efficiency up to 35%. Last but not least, a linear growth rate in the FWM efficiency is demonstrated as the strength of Fano-type interference increases in presence of the continuum states, which can be maintained for a certain propagation distance (i.e., 50μm).

Our proposed SQW structure includes a deep well and a shallow well, as illustrated in Fig. 1. The left shallow well and right deep well may be made by an $Al_{0.07}Ga_{0.93}As$ layer on the GaAs layer, separated by a $Al_{0.32}Ga_{0.68}As$ potential barrier. In general, one can obtain the eigenenergies for the four conduction subbands by solving the effective mass Schrödinger equations. The energies of two ground subbands $|1\rangle$ and $|2\rangle$ are assumed to be $E_1 = 51.53$ meV and $E_2 = 97.78$ meV, respectively. Two closely spaced delocalized subbands $|3\rangle$ and $|4\rangle$, with the eigenenergies $E_3 = 191.3$ meV and $E_4 = 233.23$ meV, are created by mixing the first excited subbands in the shallow well $|se\rangle$ and in the deep well $|de\rangle$ through the resonant tunneling. The subbands $|3\rangle$ and $|4\rangle$ can be represented by a coherent superposition of the first excited subbands in shallow and deep wells [17–19]. They are $|3\rangle = (|se\rangle - |de\rangle)/\sqrt{2}$ and $|4\rangle = (|se\rangle + |de\rangle)/\sqrt{2}$. In Fig. 1, the dashed-lines represent the corresponding energies; while the solid-curves show the wave functions for four subbands. This SQW system is driven by two continuous-wave (cw) pump laser, with the central frequency $\omega_{c1,c2}$ and wavevector $k_{c1,c2}$. Simultaneously, a weak probe pulse with the central frequency ω_p and wavevector k_p, and a FWM pulse field with the central frequency ω_m and wavevector k_m construct the wave-mixing process $|1\rangle \to |3\rangle \to |2\rangle \to |4\rangle \to |1\rangle$.

To simplify the physical picture, in the following analysis, we assume that all the subbands have the same effective mass. The SQW structure is also designed with a low electron sheet

#223802 - $15.00 USD Received 26 Sep 2014; revised 26 Oct 2014; accepted 2 Nov 2014; published 14 Nov 2014

density, in order to neglect the electron-electron interactions. In the interaction picture, with the rotating-wave approximation and the electric-dipole approximation, the interaction Hamiltonian of this system can be written as ($\hbar = 1$):

$$\begin{aligned} H_{\rm int}^{I} &= \Delta_{c1}\left|2\right\rangle\left\langle 2\right| + \Delta_{p}\left|3\right\rangle\left\langle 3\right| + \Delta_{c2}\left|4\right\rangle\left\langle 4\right| - (\Omega_{p}e^{ik_{p}\cdot r}\left|3\right\rangle\left\langle 1\right| + \Omega_{c1}e^{ik_{c1}\cdot r}\left|3\right\rangle\left\langle 2\right| \\ &+ \Omega_{c2}e^{ik_{c2}\cdot r}\left|4\right\rangle\left\langle 2\right| + \Omega_{m}e^{ik_{m}\cdot r}\left|4\right\rangle\left\langle 1\right| + H.c.), \end{aligned} \tag{1}$$

where the detuning frequencies are defined as $\Delta_p = (E_3 - E_1) - \omega_p$, $\Delta_{c1} = (E_2 - E_1) - (\omega_p - \omega_{c1})$, and $\Delta_{c2} = (E_4 - E_1) - (\omega_p - \omega_{c1} + \omega_{c2})$, respectively. The corresponding one-half Rabi frequency for the relevant laser-driven intersubband transitions is denoted as $\Omega_n\,(n = p, c1, c2, m)$. Explicitly, they are $\Omega_p = \mu_{31}E_p/2\hbar$, $\Omega_{c1} = \mu_{32}E_{c1}/2\hbar$, $\Omega_{c2} = \mu_{24}E_{c2}/2\hbar$, and $\Omega_m = \mu_{41}E_m/2\hbar$, with μ_{ij} $(i, j = 1-4;\ i \neq j)$ denoting the transition dipole moment between subbands $|i\rangle \leftrightarrow |j\rangle$ and $E_{p,c1,c2,m}$ being the slowly varying electric field amplitude of the corresponding fields.

The state wave function is assumed to be in the form of $|\Psi\rangle = A_1|1\rangle + A_2 e^{i\left(k_p - k_{c1}\right)\cdot r}|2\rangle + A_3 e^{ik_p\cdot r}|3\rangle + A_4 e^{i\left(k_p - k_{c1} + k_{c2}\right)\cdot r}|4\rangle$, where $A_j\,(j = 1,2,3,4)$ means the time-dependent probability amplitude for finding particles in the corresponding subband. Then, we substitute $|\Psi\rangle$ into the Schrödinger equation $i\partial\Psi/\partial t = H_{\rm int}^{I}\Psi$, and have the equation for the probability amplitudes,

$$i\frac{\partial A_1}{\partial t} = -\Omega_p{}^{*}A_3 - \Omega_m{}^{*}e^{i\delta k\cdot r}A_4, \tag{2}$$

$$i\frac{\partial A_2}{\partial t} = \Delta_{c1}A_2 - i\gamma_2 A_2 - \Omega_{c1}{}^{*}A_3 - \Omega_{c2}{}^{*}A_4, \tag{3}$$

$$i\frac{\partial A_3}{\partial t} = \Delta_p A_3 - i\gamma_3 A_3 - \Omega_p A_1 - \Omega_{c1}A_2 + i\zeta A_4, \tag{4}$$

$$i\frac{\partial A_4}{\partial t} = \Delta_{c2}A_4 - i\gamma_4 A_4 - \Omega_{c2}A_2 - \Omega_m e^{-i\delta k\cdot r}A_1 + i\zeta A_3. \tag{5}$$

Here, $\delta k = k_p - k_{c1} + k_{c2} - k_m$ denotes a phase mismatching factor. We also include the decay rates γ_i phenomenologically in the above equations. The total decay rates are given by $\gamma_i\,(i = 1-4) = \gamma_{il} + \gamma_{id}$, where the population decay rates γ_{il} are primarily due to the longitudinal optical phonon emission events at low temperature and the pure dipole dephasing rates γ_{id} are assumed to be a combination of quasi-elastic interface roughness scattering or acoustic phonon scattering. The population decay rates γ_{il} can be calculated [19]: upon solving the effective mass Schrödinger equation with outgoing waves at infinity, we obtain a set of complex eigenvalues whose real and imaginary parts yield respectively, the quasibound state energy levels and resonance widths. We should note that the population decay rates γ_{3l} and γ_{4l} are assumed to be the decay rates from the subbands $|3\rangle$ and $|4\rangle$ to the continuum by tunneling in the presence of the electronic continuum. When the electronic continuum is not included in the asymmetric double SQW structure, the population decay rates γ_{3l} and γ_{4l} are assumed to be the decay rates from the subbands $|3\rangle$ and $|4\rangle$ to the lower states. For the present asymmetric double quantum well structure, the population decay rates turn out to be $\gamma_{3l} = 1.58$meV, $\gamma_{4l} = 1.5$meV in presence of the electronic continuum, while the population decay rates are $\gamma_{3l} \approx \gamma_{4l} = 1$meV in absence of the electronic continuum. For the temperatures up to 10 K, the electric density may be kept as low as $10^{24}\mathrm{m}^{-3}$ [17]. In this scenario, the dephasing rates can be estimated to be $\gamma_{3d} = 0.32$meV, $\gamma_{4d} = 0.3$meV. A comprehensive treatment of the decay rates would involve incorporation of the decay mechanisms in the Hamiltonian of the system. However, we have adopted the phenomenological approach of treating the decay mechanisms just as those done in Refs. [23–26]. It is worth to be noted that a cross coupling term between the excited states

#223802 - $15.00 USD Received 26 Sep 2014; revised 26 Oct 2014; accepted 2 Nov 2014; published 14 Nov 2014

$|3\rangle$ and $|4\rangle$ is introduced by $\zeta = \sqrt{\gamma_{3l} \cdot \gamma_{4l}}$ [17–19] in the presence of the electronic continuum. We remark that $p = \zeta / \sqrt{\gamma_3 \cdot \gamma_4}$ represents the strength of Fano-type interference, for which the values $p = 0$ and $p = 1$ correspond to no interference and perfect interference, respectively.

In the limit of slowly varying amplitude approximation, the input probe pulse and the generated FWM field propagate along the "z" direction (i.e., $\delta k \cdot r = \delta k \cdot z$) according to the 1D wave equations:

$$\frac{\partial \Omega_p}{\partial z} + \frac{1}{c}\frac{\partial \Omega_p}{\partial t} = i\kappa_p A_3 A_1{}^*, \tag{6}$$

$$\frac{\partial \Omega_m}{\partial z} + \frac{1}{c}\frac{\partial \Omega_m}{\partial t} = i\kappa_m A_4 A_1{}^*, \tag{7}$$

where we have assumed $\delta k = 0$ for the sake of simplicity. The parameters $\kappa_p = 2\pi \mathrm{N}\omega_\mathrm{p}|\mu_{31}|^2/\hbar c$ and $\kappa_m = 2\pi \mathrm{N}\omega_\mathrm{m}|\mu_{41}|^2/\hbar c$ are the propagation constants, and the electron concentration in SQW is denoted by N.

In principle, above equations of probability amplitude shown in Eqs. (2)–(5) must be solved simultaneously with Maxwell's equation shown in Eqs. (6)–(7) in a self-consistent manner. Before solving those nonlinear equations, let us first examine the linear excitation of the system, which provides useful hints for the weak nonlinear theory. As a weak perturbation, we assume that the Rabi frequencies of the probe pulse and FWM field, $2\Omega_{p,m}$, are much smaller than that of the cw pump fields $2\Omega_{c1,c2}$. When the electrons are initially populated in the ground state, $|1\rangle$ (i.e., $A_1 \simeq 1$), on can perform the Fourier transformations for Eqs. (2)–(7) by defining

$$A_j(t) = \frac{1}{\sqrt{2\pi}} \int_{-\infty}^{\infty} a_j(\omega) \exp(-i\omega t) d\omega, \quad j = 2,3,4 \tag{8}$$

$$\Omega_{p,m}(t) = \frac{1}{\sqrt{2\pi}} \int_{-\infty}^{\infty} \Lambda_{p,m}(\omega) \exp(-i\omega t) d\omega, \tag{9}$$

with the Fourier transform variable ω. Then Eqs. (2)–(7) become

$$(\omega - \Delta_{c1} + i\gamma_2) a_2 + \Omega_{c1}{}^* a_3 + \Omega_{c2}{}^* a_4 = 0, \tag{10}$$

$$(\omega - \Delta_p + i\gamma_3) a_3 + \Omega_{c1} a_2 - i\zeta a_4 = -\Lambda_p, \tag{11}$$

$$(\omega - \Delta_{c2} + i\gamma_4) a_4 + \Omega_{c2} a_2 - i\zeta a_3 = -\Lambda_m, \tag{12}$$

$$\frac{\partial \Lambda_p}{\partial z} - i\frac{\omega}{c}\Lambda_p = i\kappa_p a_3 a_1{}^*, \tag{13}$$

$$\frac{\partial \Lambda_m}{\partial z} - i\frac{\omega}{c}\Lambda_m = i\kappa_m a_4 a_1{}^*, \tag{14}$$

where a_j and $\Lambda_{p,m}$ are the Fourier transforms of A_j and $\Omega_{p,m}$, respectively. The solutions for Eqs. (10)–(14) can be derived as:

$$a_2 = -\frac{i\zeta\Omega_{c1}^*\Lambda_m + (\omega - \Delta_{c2} + i\gamma_4)\Omega_{c1}^*\Lambda_p + i\zeta\Omega_{c2}^*\Lambda_p + (\omega - \Delta_p + i\gamma_3)\Omega_{c2}^*\Lambda_m}{D(\omega)}, \tag{15}$$

$$a_3 = \frac{-D_P(\omega)}{D(\omega)}\Lambda_p + \frac{D_1(\omega)}{D(\omega)}\Lambda_m, \tag{16}$$

$$a_4 = \frac{-D_m(\omega)}{D(\omega)}\Lambda_m + \frac{D_2(\omega)}{D(\omega)}\Lambda_P. \tag{17}$$

Here, we have defined shorthanded notations: $D_1(\omega)$, $D_2(\omega)$, $D_p(\omega)$, $D_m(\omega)$, and $D(\omega)$, which have the forms $D_1(\omega) = i\zeta(\omega - \Delta_{c1} + i\gamma_2) + \Omega_{c1}\Omega_{c2}^*$, $D_2(\omega) = i\zeta(\omega - \Delta_{c1} + i\gamma_2) + \Omega_{c2}\Omega_{c1}^*$,

#223802 - $15.00 USD Received 26 Sep 2014; revised 26 Oct 2014; accepted 2 Nov 2014; published 14 Nov 2014

$D_p(\omega) = |\Omega_{c2}|^2 - (\omega - \Delta_{c1} + i\gamma_2)(\omega - \Delta_{c2} + i\gamma_4)$, $D_m(\omega) = |\Omega_{c1}|^2 - (\omega - \Delta_{c1} + i\gamma_2)(\omega - \Delta_p + i\gamma_3)$, and $D(\omega) = -\zeta^2(\omega - \Delta_{c1} + i\gamma_2) - (\omega - \Delta_{c1} + i\gamma_2)(\omega - \Delta_p + i\gamma_3)(\omega - \Delta_{c2} + i\gamma_4) + i\zeta\Omega_{c2}\Omega_{c1}^* + (\omega - \Delta_{c2} + i\gamma_4)|\Omega_{c1}|^2 + i\zeta\Omega_{c1}\Omega_{c2}^* + (\omega - \Delta_p + i\gamma_3)|\Omega_{c2}|^2$, respectively.

With the given initial conditions for the probe pulse and FWM field, i.e., $\Lambda_p(0,\omega)$ and $\Lambda_m(0,\omega) = 0$, we can have the analytic solutions for these two weak fields:

$$\Lambda_p(z,\omega) = \Lambda_p(0,\omega)\left(U_+(\omega)e^{izK_+(\omega)} - U_-(\omega)e^{izK_-(\omega)}\right), \tag{18}$$

$$\Lambda_m(z,\omega) = \Lambda_p(0,\omega)S(\omega)\left(e^{izK_-(\omega)} - e^{izK_+(\omega)}\right), \tag{19}$$

where

$$K_\pm(\omega) = \frac{\omega}{c} - \frac{D_m(\omega)\kappa_m + D_p(\omega)\kappa_p \pm \sqrt{G(\omega)}}{2D(\omega)} = K_\pm(0) + K_\pm^{(1)}(\omega) + O\left(\omega^2\right), \tag{20}$$

$$U_\pm(\omega) = \frac{D_p(\omega)\kappa_p - D_m(\omega)\kappa_m \pm \sqrt{G(\omega)}}{2\sqrt{G(\omega)}} = U_\pm(0) + O(\omega), \tag{21}$$

$$S(\omega) = \frac{\kappa_m D_2(\omega)}{\sqrt{G(\omega)}} = S(0) + O(\omega), \tag{22}$$

with $G(\omega) = (D_p(\omega)\kappa_p - D_m(\omega)\kappa_m)^2 + 4D_1(\omega)D_2(\omega)\kappa_m\kappa_p$. $\Lambda_{p,m}(0,\omega)$ are the initial conditions for the pulsed probe and generated FWM fields at the entrance of the SQW structures $z = 0$. In addition, it is noted that there exist two modes ($K_\pm$ modes) described by the linearized dispersion relations $K = K_+(\omega)$ and $K = K_-(\omega)$, respectively. Typically, one can expand the dispersion relation around the center frequencies of the probe pulse and FWM field; that is, $\omega = 0$. In the following, we also neglect higher-order terms, i.e., $O\left(\omega^2\right)$ in $K_\pm(\omega)$ and $O(\omega)$ in $S(\omega)$. In general, $\mathrm{Re}[K_\pm(0)]$ and $\mathrm{Im}[K_\pm(0)]$ represent the phase shifts and absorption coefficients per unit length, respectively. The group velocities ($V_{g\pm}$) for $K_\pm$ modes are given by $1/\mathrm{Re}[K_\pm^{(1)}]$. Then, by applying an inverse Fourier transform to $\Lambda_{p,m}$, we have

$$\Omega_{p,m}(z,t) = \frac{1}{\sqrt{2\pi}}\int_{-\infty}^{\infty}\exp(-i\omega t)\Lambda_{p1,p2}(z,\omega)d\omega, \tag{23}$$

and arrive at the linearized results for the probe pulse and FWM field:

$$\Omega_p(z,t) = \Omega_p(0,\eta_+)U_+(0)e^{izK_+(0)} - \Omega_p(0,\eta_-)U_-(0)e^{izK_-(0)}, \tag{24}$$

$$\Omega_m(z,t) = S(0)\left(\Omega_p(0,\eta_-)e^{izK_-(0)} - \Omega_p(0,\eta_+)e^{izK_+(0)}\right). \tag{25}$$

Here, $\eta_\pm = t - z/V_{g\pm}$ and $\Omega_p(t) \equiv \Omega_p(z=0,t)$ is the initial probe pulse at $z = 0$. The expressions shown in Eqs. (24)–(25) give the propagation dynamics for the probe pulse and the generated FWM field in our proposed SQW system, based on which we use practical parameters to demonstrate examples to enhance FWM signals via Fano-type interference.

For the temperatures up to 10 K, the electric density may be kept as low as $10^{24}\mathrm{m}^{-3}$ [17]. In this scenario, the dephasing rates can be estimated to be $\gamma_{3d} = 0.32\mathrm{meV}$, $\gamma_{4d} = 0.3\mathrm{meV}$. The population decay rates are calculated by solving effective mass Schrödinger equation. For our QWs with continuum considered above, the population decay rates turn out to be $\gamma_{2l} = 2.36\times10^{-6}\mu\mathrm{eV}$, $\gamma_{3l} = 1.58\mathrm{meV}$, $\gamma_{4l} = 1.5\mathrm{meV}$, while the other set of decay parameters without continuum are $\gamma_{3l} = \gamma_{4l} = 1\mathrm{meV}$. As a result, we obtain $p = 0$ and $p = 0.83$ for the strength of Fano-type interference represent without and with continuum states, respectively. In addition, we choose $\Delta_{c1} = 1\mathrm{meV}$, $\Delta_p = \Delta_{c2} = 0$, and $\kappa_m = \kappa_p = 9.6\times10^3\mu m^{-1}\mathrm{meV}$.

#223802 - $15.00 USD Received 26 Sep 2014; revised 26 Oct 2014; accepted 2 Nov 2014; published 14 Nov 2014

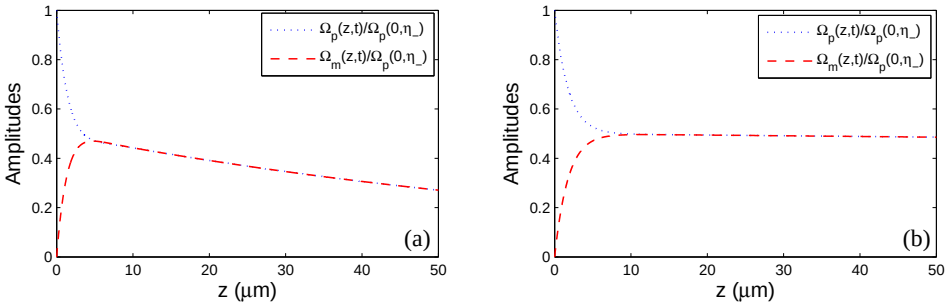

Fig. 2. Amplitudes of the probe pulse and the generated FWM field shown as a function of the depth z when penetrating into the SQW system (a) without including continuum states: $\gamma_{3l} = \gamma_{4l} = 1$meV and $p = 0$; (b) with including continuum states: $\gamma_{3l} = 1.58$meV, $\gamma_{4l} = 1.5$meV, and $p = 0.83$. Other parameters used are $\gamma_2 = 2.36 \times 10^{-6}\mu$eV, $\gamma_{3d} = 0.32$meV, $\gamma_{4d} = 0.3$meV, $|\Omega_{c1}| = 20$ meV, $|\Omega_{c2}| = 20$ meV, $\Delta_{c1} = 1$meV, $\Delta_p = \Delta_{c2} = 0$, and $\kappa_m = \kappa_p = 9.6 \times 10^3 \mu m^{-1}$meV, respectively.

Within this practical parameter set, we plot in Fig. 2 the amplitudes of probe and FWM pulses as a function of the propagation distance z for the cases (a) without and (b) with continuum states. From Fig. 2, one can find that the amplitude of probe pulse decreases monotonically as the propagation distance z increases; while the generated FWM field increases monotonically. Subsequently, after a critical propagation distance, the amplitudes of probe pulse and FWM field reach the same value. This can be explained by using the multiphoton quantum destructive interference, through the coupling excitation pathway $|1\rangle \rightarrow |3\rangle$ and the feedback excitation pathway $|1\rangle \rightarrow |3\rangle$ mediated by $|4\rangle$ [8]. Moreover, compared to the absence of continuum sates, as shown in Fig. 2(a), the amplitude remains unchanged with the introduction of the continuum sates, as shown in Fig. 2(b). Above interesting results come from the Fano-type interference caused by tunneling from the excited subbands to the continuum. This interference modifies the neighboring transitions and thus affects the multiphoton quantum destructive interference between the two different coupling pathways. When the amplitudes of probe pulse and FWM field reach the same value, the feedback excitation pathway to the subband $|4\rangle$ becomes important, which is π out of phase with respect to the coupling excitation pathway. These processes simultaneously lead to the suppression for the subband $|3\rangle$. As the propagation distance z increases, the amplitudes of $|3\rangle$ and $|4\rangle$ sacrifice from the absorption, resulting in the decay shown in Fig. 2(a). However, the decay in the amplitudes $\Omega_{m,p}$ can be suppressed, with the existence of a Fano-type interference, as shown in Fig. 2(b). As a matter of fact, this is a consequence from the competition between the destructive quantum coherence in the multiphoton interference and the constructive quantum coherence in the Fano-type interference.

According to Eqs. (24)– (25), both K_+ and K_- modes will simultaneously be excited in the SQW medium even only with one input field. However, there exists some parameter regimes where one of the two modes always decays much faster than the other. In Fig. 3, we show one example that the absorption coefficients $\alpha_\pm = \mathrm{Im}[K_\pm(0)]$ differ significantly. Here, the ratio between two absorption coefficients $\alpha_-/\alpha_+ = \mathrm{Im}[K_-(0)]/\mathrm{Im}[K_+(0)]$ is plotted versus the amplitude in the cw pump field $|\Omega_{c2}|$ for different control field amplitudes $|\Omega_{c1}|$ in the absence of the electronic continuum, see Fig. 3(a). In order to examine the effect of Fano-type interference on the absorption coefficients, we plot in Fig. 3(b) the ratio α_-/α_+ versus the amplitude in the cw pump field $|\Omega_{c2}|$ with and without including the continuum states. It can be obviously found that the absorption coefficient ratio decreases as the amplitudes of two pump

#223802 - $15.00 USD Received 26 Sep 2014; revised 26 Oct 2014; accepted 2 Nov 2014; published 14 Nov 2014

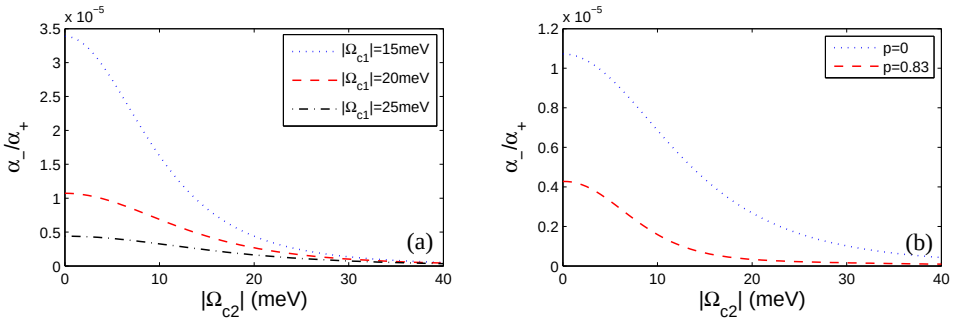

Fig. 3. The ratio between absorption coefficients α^-/α^+ for two different modes shown as a function of the amplitude $|\Omega_{c2}|$ in the cw control field $c2$: (a) for different control field amplitudes $|\Omega_{c1}|$ in the absence of the continuum state and (b) for different case, i.e., without or with including the continuum sate for a fixed value of $|\Omega_{c1}| = 20$ meV. Without continuum states ($p = 0$): $\gamma_{3l} = \gamma_{4l} = 1$meV; with continuum states ($p = 0.83$): $\gamma_{3l} = 1.58$meV and $\gamma_{4l} = 1.5$meV. Other parameters used are $\gamma_2 = 2.36 \times 10^{-6}\mu$eV, $\gamma_{3d} = 0.32$meV, $\gamma_{4d} = 0.3$meV, $\Delta_{c1} = 1$meV, $\Delta_p = \Delta_{c2} = 0$, and $\kappa_m = \kappa_p = 9.6 \times 10^3 \mu m^{-1}$meV, respectively.

fields increase. Moreover, even for $p = 0.83$ in presence of the continuum state, we have $\alpha_- \ll \alpha_+$. In other words, Fig. 3 illustrates that the K_+ mode decays much more quickly than the K_- mode. Thus, one can safely neglect this faster variable K_+ after a characteristic propagation distance. As a consequence, the two weak pulses propagate with the matched group velocity $V_g = V_{g-}$. By neglecting the K_+ mode, the probe and FWM pulses $\Omega_{p,m}$ can be rewritten as

$$\Omega_p(z,t) = -\Omega_p(0, t - z/V_g)\, U_-(0)\, e^{iz\beta - z\alpha}, \tag{26}$$

$$\Omega_m(z,t) = S(0)\Omega_p(0, t - z/V_g)\, e^{iz\beta - z\alpha}, \tag{27}$$

where $V_g = V_{g-} = 1/\mathrm{Re}[K_-^{(1)}]$ is the group velocity, $\alpha = \mathrm{Im}[K_-(0)]$ denotes the absorption coefficient, and $\beta = \mathrm{Re}[K_-(0)]$ represents the phase shift per unit length. Based on Eqs. (26)–(27), one can see that the probe pulse and the generated FWM field travel at a ultraslow group velocity.

In Fig. 4, we plot the group velocity V_g/c as a function of pump field amplitude $|\Omega_{c2}|$ for different sets of cw amplitude $|\Omega_{c1}|$. The group velocity exhibits the similar trends for different case, i.e., with or without continuum states. However, in the presence of the continuum states ($p = 0.83$), the slower group velocity can be achieved, i.e., on the order of $10^{-4}c$ as shown in Fig. 4(b). It should be noted that a further reduced group velocity can be obtained by choosing the related parameter values appropriately.

As illustrated in Fig. 3 and Fig. 4, the probe pulse and the generated FWM field can travel through the SQW medium with the same temporal profile and at a ultraslow group velocity within a characteristic distance. Now, we turn to the conversion efficiency for the FWM field. Based on the definition in Ref. [27], the efficiency for the generated FWM field can be measured as $\rho = \left| E_m^{(out)}/E_p^{(in)} \right|^2$, where $E_m^{(out)}$ is the electric field E_m $\left(|E_m|^2 = 4\hbar^2 |\Omega_m|^2/|\mu_{31}|^2 \right)$ for the generated FWM field at the exit $z = L$ and $E_p^{(in)}$ $\left(|E_p|^2 = 4\hbar^2 |\Omega_p|^2/|\mu_{31}|^2 \right)$ is the electric field for the probe pulse at the entrance $z = 0$. According to Eqs. (26) – (27), the efficiency for FWM

#223802 - $15.00 USD Received 26 Sep 2014; revised 26 Oct 2014; accepted 2 Nov 2014; published 14 Nov 2014

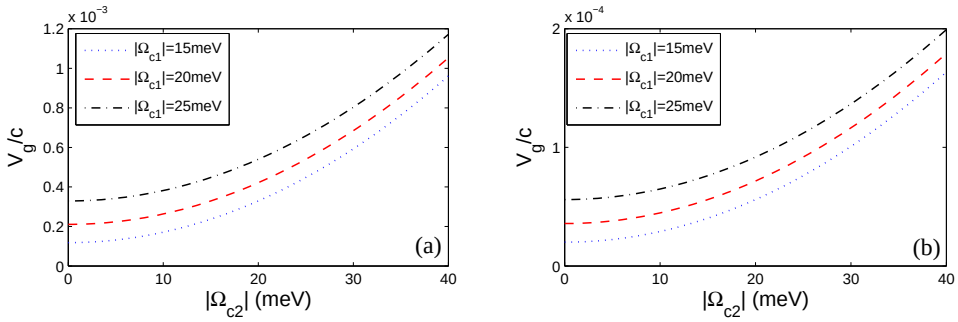

Fig. 4. Relative group velocity V_g/c versus the cw amplitude Ω_{c2} for different pump fields $|\Omega_{c1}|$, (a) without including continuum states: $\gamma_{3l} = \gamma_{4l} = 1$meV and $p = 0$; and (b) with including continuum states: $\gamma_{3l} = 1.58$meV, $\gamma_{4l} = 1.5$meV, and $p = 0.83$. Other parameters used are $\gamma_2 = 2.36 \times 10^{-6}\mu$eV, $\gamma_{3d} = 0.32$meV, $\gamma_{4d} = 0.3$meV, $\Delta_{c1} = 1$meV, $\Delta_p = \Delta_{c2} = 0$, and $\kappa_m = \kappa_p = 9.6 \times 10^3 \mu m^{-1}$meV, respectively.

signal has the form,

$$\rho = \left(\frac{E_m}{E_p}\right)^2 = \frac{|\mu_{31}|^2}{|\mu_{41}|^2} \frac{\kappa_m^2 (B)^2}{4\kappa_m \kappa_p (B)^2 + (A)^2} e^{-2\alpha L}, \tag{28}$$

with $A = \kappa_m |\Omega_{c1}|^2 - \kappa_p |\Omega_{c2}|^2 + i\kappa_m \Delta_{c1}\gamma_3 + \kappa_m \gamma_2 \gamma_3 - i\kappa_p \Delta_{c1}\gamma_4 - \kappa_p \gamma_2 \gamma_4$, and $B = \Omega_{c2}\Omega_{c1}^* - i\zeta\Delta_{c1} - \zeta\gamma_2$. By means of the relation $\mu_{31}^2/\mu_{41}^2 = \kappa_p \omega_m / \kappa_m \omega_p$, it is found that the FWM efficiency ρ can have a simple form, $\rho = \left(\omega_m \cdot e^{-2\alpha L}\right)/(4\omega_p)$.

To study the dependence on different system parameters for the generated FWM efficiency, first of all, we analyze how the amplitude of cw pump fields modifies the conversion efficiency in Fig. 5. Here, the FWM efficiency ρ is plotted as a function of the amplitude Ω_{c2} of the cw pump field $c2$, for the different cw pump fields $c1$ without and with including the continuum states, shown in Fig. 5(a) and 5(b), respectively. One can see that the amplitude of two cw pump fields and the Fano-type interference caused by the tunneling from the excited subbands to the continuum both have an obvious influence on the FWM conversion efficiency. Moreover, a maximum value in the FWM conversion efficiency can be achieved when $|\Omega_{c1}| = |\Omega_{c2}|$. In our simulations, even for a deep penetration distance into the SQW structure, such as $L = 6\mu$m, one can still have the conversion efficiency up to $\rho > 35\%$. Direct comparison in Figs. 5(a) and (b) implies that the maximum value in the conversion efficiency can be enhanced when the continuum states are included. In other words, the Fano-type interference results from the resonant tunneling from the excited subbands to the continuum opens the channel for the FWM process. Different from previous FWM schemes based on EIT configuration, parameters for the electronic subbands in SQW systems can be engineered to give a desired strength of interference by utilizing the so-called structure coherent control in design [17].

To give a better insight on the FWM conversion efficiency from the amplitudes of two cw pump fields, in Fig. 6, we show the conversion efficiency ρ as a function of the amplitudes in two cw pump fields $|\Omega_{c1}|/|\Omega_{c2}|$ without including the continuum states. The results shown in Fig. 6 clearly verify that the condition to achieve a maximum efficiency happens around $|\Omega_{c1}| = |\Omega_{c2}|$. Although, for the same amplitudes of two cw pump fields the highly efficiency can be obtained, the extent of the robustness is small. In the presence of the Fano-type interference caused by tunneling from the excited subbands to the continuum, in Fig. 7, we show the conversion efficiency ρ as a function of the strength of the Fano-type interference p for the different amplitudes of two pump fields. For simplicity, here we have assumed the popu-

#223802 - $15.00 USD Received 26 Sep 2014; revised 26 Oct 2014; accepted 2 Nov 2014; published 14 Nov 2014

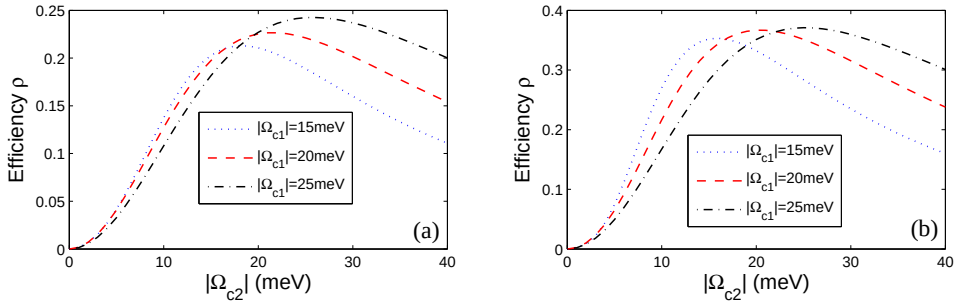

Fig. 5. FWM conversion efficiency ρ versus the amplitude $|\Omega_{c2}|$ for different cw pump fields: $|\Omega_{c1}| = 15$meV, $|\Omega_{c1}| = 20$meV, $|\Omega_{c1}| = 25$meV, (a) without including continuum states: $\gamma_{3l} = \gamma_{4l} = 1$meV and $p = 0$; and (b) with including continuum states: $\gamma_{3l} = 1.58$meV, $\gamma_{4l} = 1.5$meV, and $p = 0.83$. Other parameters used are $L = 6\mu m$, $\gamma_2 = 2.36 \times 10^{-6}\mu$eV, $\gamma_{3d} = 0.32$meV, $\gamma_{4d} = 0.3$meV, $\Delta_{c1} = 1$meV, $\Delta_p = \Delta_{c2} = 0$, and $\kappa_m = \kappa_p = 9.6 \times 10^3 \mu m^{-1}$meV, respectively.

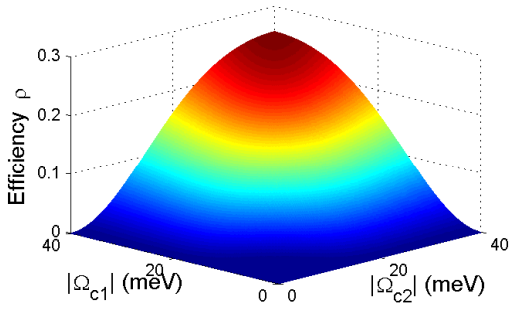

Fig. 6. The conversion efficiency ρ for the generated FWM field as a function of the amplitude of two cw pump fields ($|\Omega_{c1}|$ and $|\Omega_{c2}|$) without including the continuum states. Other parameters used are $p = 0$, $L = 6\mu m$, $\gamma_2 = 2.36 \times 10^{-6}\mu$eV, $\gamma_{3l} = \gamma_{4l} = 1$meV, $\gamma_{3d} = 0.32$meV, $\gamma_{4d} = 0.3$meV, $\Delta_{c1} = 1$meV, $\Delta_p = \Delta_{c2} = 0$, and $\kappa_m = \kappa_p = 9.6 \times 10^3 \mu m^{-1}$meV, respectively.

lation decay rates from subbands $|3\rangle$ and $|4\rangle$ to the continuum states remain unchanged (i.e., $\gamma_{3l} = 1.58$ meV and $\gamma_{4l} = 1.5$ meV), and the different values of interference strength p can be obtained by varying total decay rates γ_3 and γ_4. Interestingly enough, as shown in Fig. 7, the conversion efficiency for the generated FWM field increases linearly as the strength of Fano-type interference increases for a certain propagation distance. It is the Fano-type interference that suppresses the population in the subbands $|3\rangle$ and $|4\rangle$, resulting in the reduction of the corresponding absorption in the generated FWM field. Again, the Fano-type interference leads to the enhancement of conversion efficiency. However, the linear increasing of the maximal conversion efficiency has robustness only in a small region of two cw pump fields intensities. As illustrated in Fig. 7, the increasing effect will be not obviously if the amplitudes of two pump fields increases continuously.

Since the probe field and the generated FWM signal are in the form of optics pulses, here, we also consider the influence of propagation distance on the relevant conversion efficiency. To do this, we assume that the probe field at the entrance of the SQW structure has a Gaussian pulse

#223802 - $15.00 USD Received 26 Sep 2014; revised 26 Oct 2014; accepted 2 Nov 2014; published 14 Nov 2014

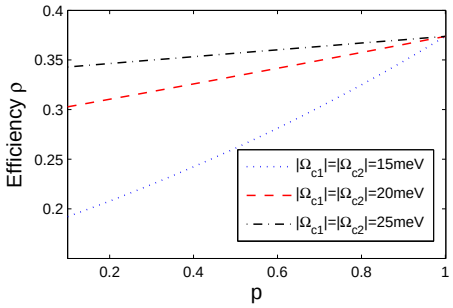

Fig. 7. (Color online) The conversion efficiency ρ for the generated FWM field as a function of the strength of the Fano-type interference p for the different amplitudes of two pump fields in presence of the continuum states. Other parameters used are $L = 6\mu m$, $\gamma_2 = 2.36 \times 10^{-6}\mu$eV, $\gamma_{3l} = 1.58$meV, $\gamma_{4l} = 1.5$meV, $\Delta_{c1} = 1$meV, $\Delta_p = \Delta_{c2} = 0$, and $\kappa_m = \kappa_p = 9.6 \times 10^3 \mu m^{-1}$meV, respectively.

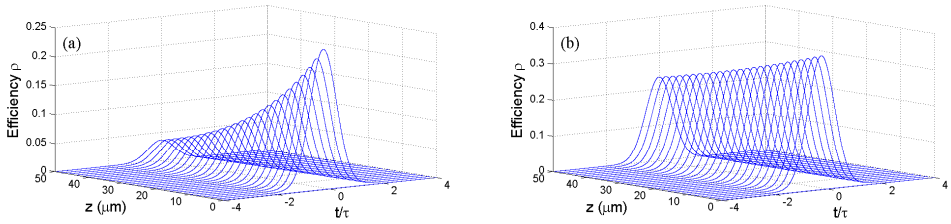

Fig. 8. Surface plot of the FWM conversion efficiency ρ as a function of the normalized time t/τ and the propagation distance z for (a) without including continuum states: $\gamma_{3l} = \gamma_{4l} = 1$meV and $p = 0$; and (b) with including continuum states: $\gamma_{3l} = 1.58$meV, $\gamma_{4l} = 1.5$meV, and $p = 0.83$. Other parameters used are $|\Omega_{c1}| = |\Omega_{c2}| = 20$ meV, $\gamma_2 = 2.36 \times 10^{-6}\mu$eV, $\gamma_{3d} = 0.32$meV, $\gamma_{4d} = 0.3$meV, $\Delta_{c1} = 1$meV, $\Delta_p = \Delta_{c2} = 0$, and $\kappa_m = \kappa_p = 9.6 \times 10^3 \mu m^{-1}$meV, respectively.

profile, i.e., $\Omega_p(0,t) = \Omega_p(0,0)e^{-(t^2/\tau^2)}$, with the pulse width τ. Now, the conversion efficiency can be rewritten as $\rho = |\Omega_m(z,t)/\Omega_p(0,0)|^2$. The results from numerical simulations for the corresponding FWM conversion efficiency are shown in Fig. 8, with the pulse width fixed as $\tau = 10$ meV $^{-1}$. It can be seen clearly that the conversion efficiency ρ decreases significantly as the propagation distance increases when the Fano-type interference caused by tunneling from the excited subbands to the continuum is not included, (a) $p = 0$; while it decreases slowly for a longer propagation distance due to the existence of the Fano-type interference when the continuum states are included, (b) $p = 0.83$. From the comparison between Fig. 8(a) and Fig. 8(b), the presence of a Fano-type interference indeed modifies not only the linear optical property, but also the FWM process. As shown in Fig. 4, the Fano-type interference contributes to slow down the matched group velocity. Consequently, such a reduced group velocity ensures a longer interaction time, and leads to maintain a higher FWM conversion efficiency for a longer propagation distance.

In conclusion, we have performed a time-dependent analysis for the four-wave mixing (FWM) process in the ultraslow propagation regime, by considering the intersubband transitions in an asymmetric semiconductor double quantum well system. By including the Fano-type interference caused by the tunneling from the excited subbands to the electronic continuum, we demonstrate an efficient way to generate FWM field by means of two continuous-wave (cw)

#223802 - $15.00 USD Received 26 Sep 2014; revised 26 Oct 2014; accepted 2 Nov 2014; published 14 Nov 2014

pump fields and a weak probe pulse. Through the Schrödinger-Maxwell formalism, we also give the corresponding analytical expressions for the input probe pulse and the generated FWM field in the linear regime under the steady-state condition. In presence of the Fano-type interference, the conversion efficiency of FWM field is revealed to be enhanced significantly, up to 35%. Take the advantages of flexibilities in semiconductor structures, our results provide a practical opportunity to implement optical modulated solid-state devices.

Acknowledgments

The research is supported in part by National Natural Science Foundation of China under Grant Nos. 11374050 and 61372102, by Qing Lan project of Jiangsu, and by the Fundamental Research Funds for the Central Universities under Grant No. 2242012R30011.

#223802 - $15.00 USD Received 26 Sep 2014; revised 26 Oct 2014; accepted 2 Nov 2014; published 14 Nov 2014